Biophys Rep 2025, 11(X):1–13
https://doi.org/10.52601/bpr.2025.250034 https://cstr.cn/32402.14.bpr.2025.250034
Biophysics Reports

RESEARCH ARTICLE

Nanobody PET tracer enables GPA33 expression profiling for precision diagnosis of colorectal cancer

Chengwen Zheng[1,2,3], Zhidie Huang[4], Shaowen Yang[1,2,3], Sixuan Cheng[1,2,3], Wenbo Li[1,2,3], Hao Yang[1,2,3], Dawei Jiang[1,2,3] ✉, Weijun Wei[5] ✉, Weibo Cai[6] ✉

[1] Department of Nuclear Medicine, Union Hospital, Tongji Medical College, Huazhong University of Science and Technology, Wuhan 430022, China
[2] Hubei Province Key Laboratory of Molecular Imaging, Wuhan 430022, China
[3] Key Laboratory of Biological Targeted Therapy, Ministry of Education, Wuhan 430022, China
[4] Department of Nuclear Medicine, The Affiliated Hospital of Inner Mongolia Medical University, Hohhot 010050, China
[5] Department of Nuclear Medicine, Institute of Clinical Nuclear Medicine, Renji Hospital, School of Medicine, Shanghai Jiao Tong University, Shanghai 200233, China
[6] Departments of Radiology, Medical Physics, and Carbone Cancer Center, University of Wisconsin – Madison, WI 53705, USA

Received: 5 June 2025 / Accepted: 22 July 2025

Abstract Colorectal cancer (CRC) remains a leading cause of cancer mortality, highlighting the need for precise molecular imaging tools targeting biomarkers like glycoprotein A33 (GPA33), which is highly expressed in over 95% of CRC but currently lacks an ideal non-invasive probe for rapid clinical translation. This study developed a GPA33-targeted nanobody tracer, [^{68}Ga]Ga-NOTA-WWH347, for PET imaging of CRC by engineering and radiolabeling a specific nanobody WWH347 with Ga-68. Western blot confirmed higher GPA33 expression in LS174T cells versus HT29 controls. *In vitro* cell uptake assays demonstrated specific tracer accumulation in LS174T cells (10.27 ± 0.45% at 2 h) versus negative HT29 cells (1.13 ± 0.14%) or LS174T blocking groups (0.96 ± 0.55%). The novel tracer [^{68}Ga]Ga-NOTA-WWH347 enabled superior PET visualization of CRC tumors in subcutaneous, liver metastasis, and systemic metastasis models, clearly outperforming both [^{18}F]F-FDG and the non-specific probe [^{68}Ga]Ga-NOTA-5D5. Subsequent biodistribution studies revealed significantly higher tracer uptake in subcutaneous LS174T tumors (10.45 ± 0.78 %ID/g) compared to HT29 (3.29 ± 0.61 %ID/g). In addition, animal models with liver metastases showed tracer uptake at 11.69 ± 2.69 %ID/g, while 9.71 ± 1.01 %ID/g in systemic metastatic lesions, enabling non-invasive visualization of GPA33 expression profiles on the whole-body level. These findings establish [^{68}Ga]Ga-NOTA-WWH347 as a precision diagnostic tool that could optimize GPA33-targeted therapies by mapping expression patterns in CRC primary tumors and metastatic lesions through rapid, specific PET imaging.

Keywords GPA33, Colorectal cancer, Nuclear medicine, Nanobody, Molecular imaging

Electronic supplementary material The online version of this article contains supplementary material, which is available to authorized users.

✉ Correspondence: daweijiang@hust.edu.cn (D. Jiang), wwei@shsmu.edu.cn (W. Wei), wcai@uwhealth.org (W. Cai)

INTRODUCTION

Colorectal cancer (CRC), representing 10% of global malignancies, ranks as the third most prevalent cancer type and second-leading cause of oncologic mortality

(Siegel *et al*. 2023). While surgical resection remains definitive for localized disease, its efficacy depends on precise preoperative delineation of tumor margins and nodal involvement to preserve physiological function (Abedizadeh *et al*. 2024; Heriot *et al*. 1999). The disease's early diagnostic challenge persists, with 35% of cases demonstrating lymph node or distant metastases at presentation, substantially limiting surgical utility (Eng *et al*. 2022; Ulintz *et al*. 2018). Despite therapeutic advancements, CRC maintains a five-year survival rate below 60%, underscoring the critical need for non-invasive biomarkers enabling early detection and metastatic surveillance to optimize therapeutic outcomes (Abakushina *et al*. 2019; Ganesh *et al*. 2019).

Protein glycoprotein A33 (GPA33), encoded by the GPA33 gene belonging to the immunoglobulin superfamily, is abundantly expressed in more than 95% of human primary and metastatic colorectal cancers, with restricted expression in normal tissues (colon and intestinal epithelium) (Garinchesa *et al*. 1996; Heath *et al*. 1997). Moreover, elevated GPA33 expression in tumor tissues has been demonstrated to be inversely correlated with patient prognosis (Lopes *et al*. 2020). Therefore, GPA33 has emerged as a promising antigen for targeted therapy in colorectal cancer, and has been extensively studied in preclinical and clinical studies (Bendell *et al*. 2014; Carrasquillo *et al*. 2011; Chong *et al*. 2005; Infante *et al*. 2013; Welt *et al*. 1996, 2003). Due to the spatial heterogeneity of GPA33, non-invasive, systemic assessment of GPA33 expression *in vivo* is critical to stratify therapeutic cohorts, longitudinally monitor treatment efficacy, and prognosticate clinical outcomes.

Conventional imaging such as ultrasonography, magnetic resonance imaging (MRI), and computed tomography (CT) imaging are widely used for cancer diagnosis, but they lack biomarker specificity (Fenster and Downey 2000; Flohr and Schmidt 2023; Schwab *et al*. 2008). Molecular imaging allows visualization, characterization, and quantification of biological processes in intact living organisms at the cellular and subcellular levels (James and Gambhir 2012). PET/CT imaging has become the clinical basis for cancer diagnosis and clinical staging of several malignant tumors (Tan *et al*. 2020). 2-[^{18}F]fluoro-2-deoxy-D-glucose ([^{18}F]F-FDG), the most commonly PET agent, is a glucose analog that can show glucose metabolism in patients and differentiate benign and malignant lesions (Ametamey *et al*. 2008; Weissleder 2006). In addition, glucose metabolism can also be increased due to infection or inflammation, allowing for some false positives for [^{18}F]F-FDG (Wang *et al*. 2014). Therefore, the development of diagnostic modalities with higher specificity and sensitivity is urgently needed.

Target-based molecular imaging with immune-positron emission tomography (immunoPET) is an innovative and attractive modality (Wei *et al*. 2020). It combines the high specificity and selectivity of antibodies (or their derivatives) with the imaging sensitivity of PET and allows for non-invasive monitoring of biomarker dynamics (Menzies and Lastoria 2022). A variety of immunoPET tracers have been extensively explored in preclinical studies, some of which are in the translational phase (Wei *et al*. 2020). Several monoclonal antibodies (mAbs) targeting GPA33 have been developed and applied in preclinical CRC models for imaging and radioimmunotherapy (Chandler *et al*. 2022; Cheal *et al*. 2016; Vaughn *et al*. 2024). Despite their clinical promise, antibody-based PET imaging requires long-lived radionuclides (*e.g.*, ^{89}Zr) to match IgG's extended half-life (7–21 days), yet limited radiopharmacy infrastructure restricts clinical accessibility (Grilo and Mantalaris 2019). Same-day immunoPET imaging using short half-life radionuclide-labelled antibody fragments of lower molecular weight can overcome this disadvantage. Nanobodies (~15 kDa) stand out due to their short biological half-life (several hours), high stability, remarkable tissue penetration, low immunogenicity and multifunctional engineering potential (Wei *et al*. 2022). In this study, we aim to engineer a novel nanobody-derived GPA33-targeting immunoPET imaging tracer and evaluate its diagnostic effectiveness across various preclinical tumor models.

RESULTS

Synthesis, radiolabeling and targeting ability of WWH347

The purity of nanobody WWH347 was >95%, assessed by the sodium dodecyl sulfate polyacrylamide gel electrophoresis (SDS-PAGE) (Fig. 1A) and high-performance liquid chromatography (HPLC) (Fig. 1D). After labelling WWH347 with ^{68}Ga, the results obtained from HPLC indicate that the radiochemical purity (RCP) of the probe is >95%. In addition, the UV chromatograms and radioactive chromatography exhibited consistency both prior to and following the labelling process, suggesting that the chemical stability of the compounds was maintained throughout the radiolabeling procedure (Figs. 1D and 1E). The RCP of the probe was >75% after 4 h incubation at 37°C in 50% FBS, which suggests that the labelled nanobody

exhibited good stability in serum (Fig. 1F and supplementary Fig. S1). Semi-quantitative analysis based on Western Blot (WB) results indicated that GPA33 expression was significantly higher in LS174T than HT29 cells (Figs. 1B and 1C). The cell uptake assay indicated that the uptake of radioactive probe [^{68}Ga]Ga-NOTA-WWH347 by LS174T cells reached 2.60 ± 0.34% at 15 min, with a gradual increase over time, and the uptake rate reached 10.27 ± 0.45% at 2 h of incubation (Fig. 1G). Notably, the uptake rate in LS174T cells was significantly diminished following the application of excess cold nanobody precursor, resulting in cell uptake of only 0.96 ± 0.55% after 2 h of incubation. The uptake rate of control HT29 cells was similar to that of the blocked group. The demonstrated cellular-level affinity and specificity of WWH347 for GPA33 warrant further *in vivo* studies.

ImmunoPET imaging in subcutaneous tumor models

The GPA33-targeting ability of [^{68}Ga]Ga-NOTA-WWH347 was initially assessed in subcutaneous LS174T CRC cell-derived xenograft (CDX) models

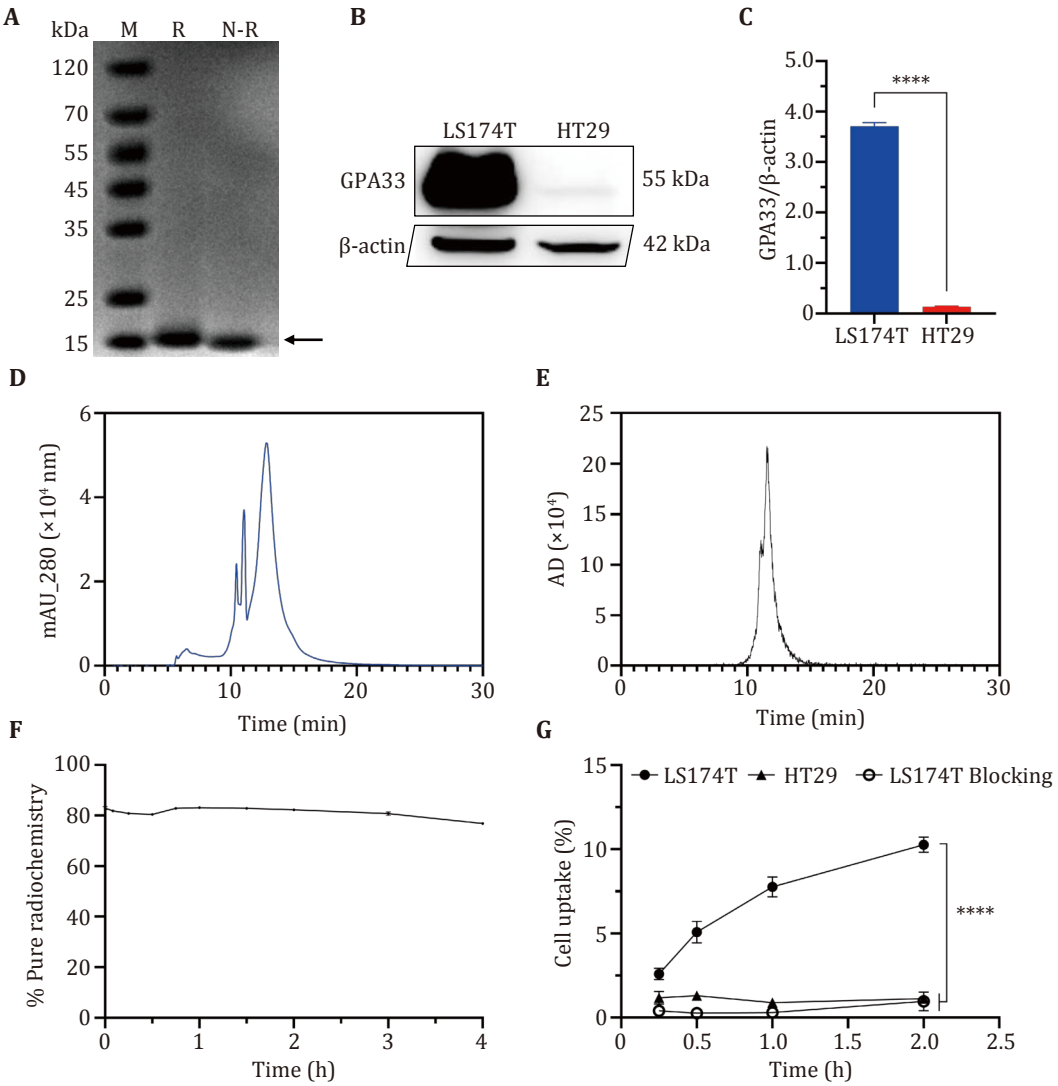

Fig. 1 Synthesis, radiolabeling and targeting ability of WWH347. **A** The SDS-PAGE analysis of WWH347. **B**,**C** The WB results of GPA33 expression in LS174T and HT29 cells. **D**,**E** The HPLC analysis of WWH347 and [^{68}Ga]Ga-NOTA-WWH347. **F** Stability analysis of [^{68}Ga]Ga-NOTA-WWH347 in 50% FBS at 37°C. **G** Cell uptake assays of [^{68}Ga]Ga-NOTA-WWH347 in LS174T, HT29 and LS174T Blocking groups. M: marker, R: reduction, N-R: non-reduction. Data are presented as the mean ± SD of three independent experiments (n = 3 per group). ****P < 0.0001 compared with the control group

(Fig. 2A). The immunoPET/CT imaging revealed that the tumor was distinctly visualized 2 h post-injection of [^{68}Ga]Ga-NOTA-WWH347. Quantitative analysis of the ROI indicated that [^{68}Ga]Ga-NOTA-WWH347 exhibited the highest accumulation in the kidneys, with a value of 267.50 ± 14.63 %ID/g, followed by the tumor, which demonstrated an uptake value of 15.35 ± 1.61 %ID/g (Fig. 2B). In addition, the quantitative data clearly demonstrate that [^{68}Ga]Ga-NOTA-WWH347 exhibits rapid and high tumor uptake, achieving significant accumulation by 15–30 min (supplementary Fig. S2). Importantly, the tracer shows excellent retention within the tumor at the 2-h time point, with only minimal washout observed. Parallel imaging was performed in the HT29 CDX models with low GPA33 expression (Fig. 2C). The tumor uptake of [^{68}Ga]Ga-NOTA-WWH347 was significantly lower, with ROI analysis indicating a tumor uptake value of 3.88 ± 0.83 %ID/g (Fig. 2D). In contrast, the non-specific nanobody ([^{68}Ga]Ga-NOTA-A50-2_5D5) failed to detect subcutaneous LS174T

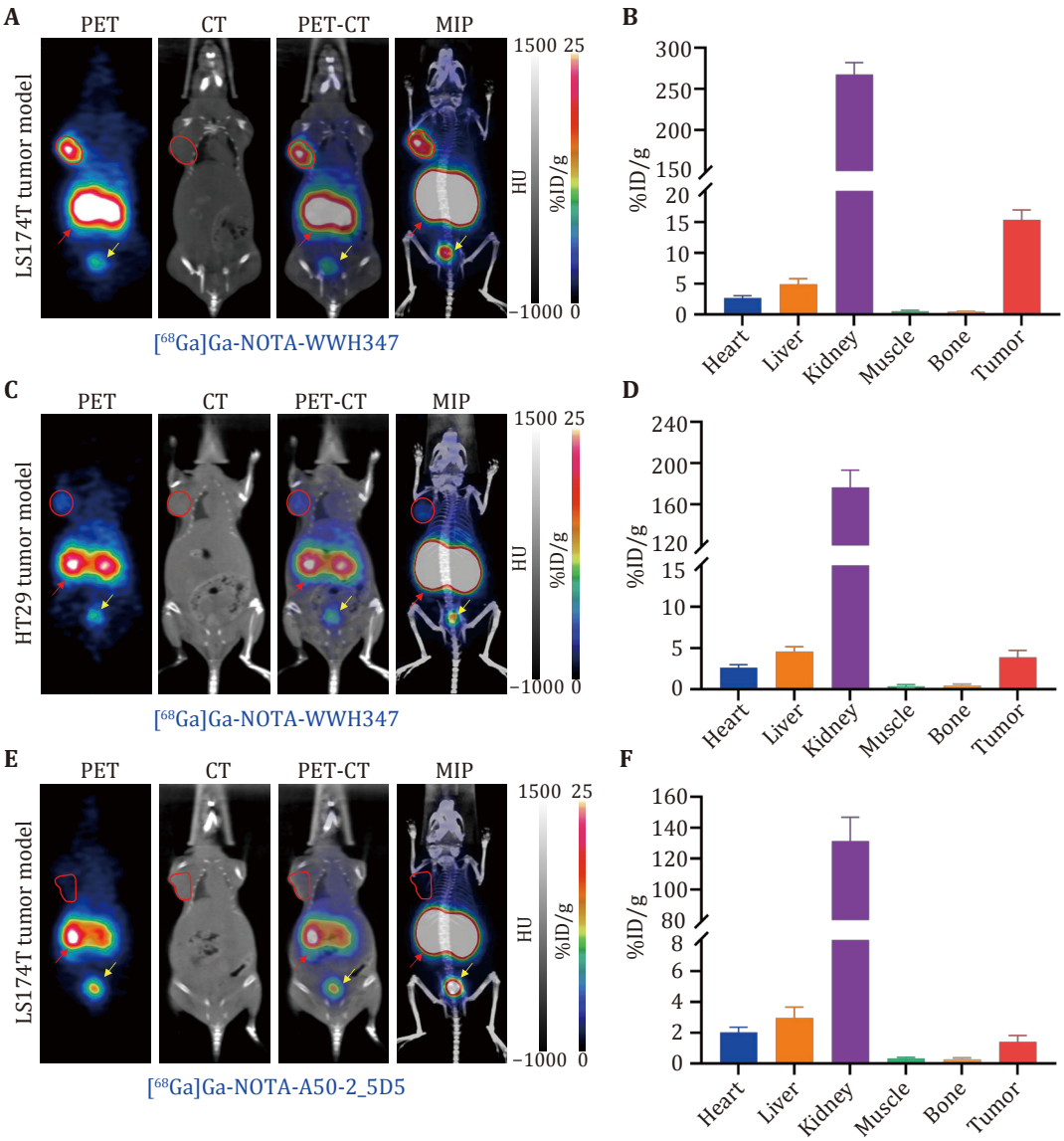

Fig. 2 ImmunoPET/CT imaging with [^{68}Ga]Ga-NOTA-WWH347 in subcutaneous CRC models. Representative images of [^{68}Ga]Ga-NOTA-WWH347 (**A**, **C**) and [^{68}Ga]Ga-NOTA-A50-2_5D5 (**E**) in subcutaneous cell-derived xenograft (CDX) mouse models with high (LS174T) and low (HT29) expression of GPA33. The subcutaneous tumors (red circles), the kidneys (red arrows) and bladders (yellow arrows) were displayed on the coronal images and MIP images. The ROI quantification results in LS174T tumor model (**B**) and HT29 tumor model (**D**) 2 h after [^{68}Ga]Ga-NOTA-WWH347 injection (**F**). ROI results of [^{68}Ga]Ga-NOTA-A50-2_5D5 in LS174T tumor model. Data were quantified as %ID/g. Quantitative analysis data were shown as mean ± SD (n = 4)

tumors (Fig. 2E), with extremely low tumor uptake of only 1.42 ± 0.41 %ID/g (Fig. 2F). Biodistribution data 2 h post-injection showed similar organ uptake trends as the ROI results (Fig. 3A). The results demonstrated the subcutaneous LS174T tumors had significantly higher uptake of [^{68}Ga]Ga-NOTA-WWH347 (10.45 ± 0.78 %ID/g) compared to the HT29 group (3.29 ± 0.61 %ID/g). In contrast, the uptake of [^{68}Ga]Ga-NOTA-A50-2_5D5 was only 0.86 ± 0.10 %ID/g in LS174T tumors. The excellent targeting ability and specificity demonstrated by WWH347 in subcutaneous models encourage us to compare its diagnostic value with the

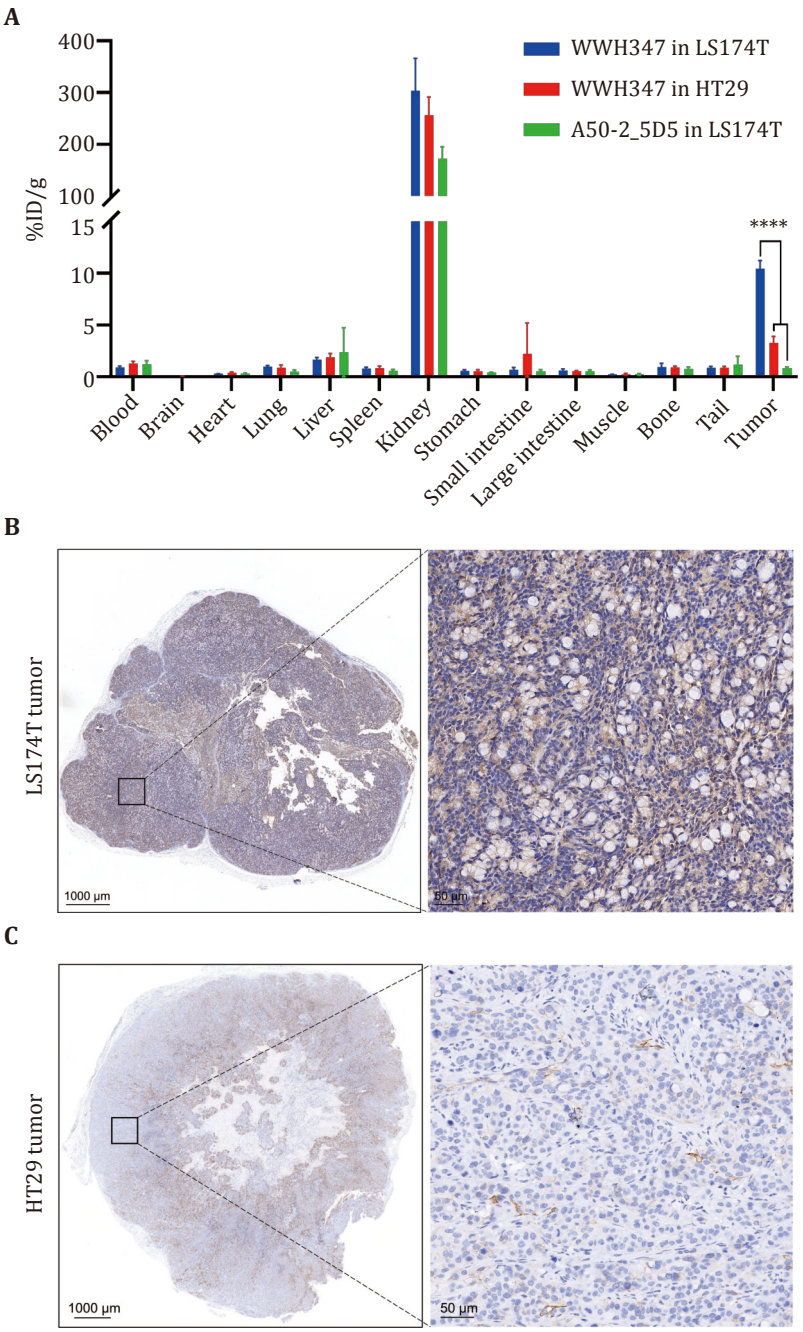

Fig. 3 *Ex vivo* biodistribution and histopathological staining results. **A** Results of biodistribution in LS174T and HT29 models after 2 h of [^{68}Ga]Ga-NOTA-WWH347 and [^{68}Ga]Ga-NOTA-A50-2_5D5 injection. **B**,**C** The GPA33 IHC staining of fixed subcutaneous LS174T and HT29 tumors. Data are presented as the mean ± SD of four independent experiments (n = 4). ****P < 0.0001 compared with the control group

most commonly used probe, [^{18}F]F-FDG (supplementary Fig. S3A). The tumor uptake of [^{18}F]F-FDG was 5.80 ± 1.41 %ID/g (supplementary Fig. S3B). The tumor uptake of [^{68}Ga]Ga-NOTA-WWH347 was significantly superior to that of [^{18}F]F-FDG, and it had a better tumor-to-muscle ratio (30.51 ± 8.89 vs 1.03 ± 0.52) (supplementary Fig. S3C). In conclusion, immunoPET imaging of [^{68}Ga]Ga-NOTA-WWH347 can be an effective diagnostic in preclinical models with high GPA33 expression. The IHC results revealed significantly higher GPA33 expression in LS174T versus HT29 tumors (Figs. 3B and 3C), correlating closely with immuno-PET imaging findings.

ImmunoPET imaging in liver metastasis tumor models

To further validate the diagnostic ability of [^{68}Ga]Ga-NOTA-WWH347 on colorectal metastasis models, we conducted the immunoPET in LS174T liver metastasis tumor models. [^{68}Ga]Ga-NOTA-WWH347 demonstrated a clear delineation of liver metastases at 2 h post-injection (Fig. 4A). To exclude the interference of high renal uptake, the mice were euthanized, and immunoPET imaging of the principal *ex vivo* organs was conducted (Fig. 4B). The results of the immunoPET imaging corresponded to the anatomical illustrations, confirming that [^{68}Ga]Ga-NOTA-WWH347 could accurately identify metastatic tumors in the liver. The ROI analysis showed that [^{68}Ga]Ga-NOTA-WWH347 has the highest uptake in the kidney at 220.15 ± 22.41 %ID/g, followed by the tumor at 21.25 ± 4.21 %ID/g (Fig. 4C). Subsequent biodistribution analysis data showed the same organ uptake trend as the ROI results, still having the highest renal accumulation of 275.39 ± 37.18 %ID/g and tumor uptake of 11.69 ± 2.69 %ID/g (Fig. 4D). The immunohistochemical analysis confirmed that GPA33 was expressed extensively on the membrane of tumor cells associated with liver metastases. The findings from the immunohistochemical assessments exhibited a strong correlation with the immuno-PET results of [^{68}Ga]Ga-NOTA-WWH347.

ImmunoPET imaging in systemic metastasis tumor models

Furthermore, we further validated the diagnostic ability of [^{68}Ga]Ga-NOTA-WWH347 for CRC micrometastases in systemic metastasis LS174T tumor models. [^{68}Ga]Ga-NOTA-WWH347 could clearly show small metastatic tumors throughout the body at 2 h after injection (Fig. 5A). The mice were euthanized and dissected (Fig. 5B). The locations of the metastatic tumors identified in the dissection images corresponded with the results of immunoPET, demonstrating that [^{68}Ga]Ga-NOTA-WWH347 has the ability to accurately and completely identify CRC micrometastases. The ROI analysis showed that [^{68}Ga]Ga-NOTA-WWH347 had the highest enrichment in the kidney at 204.82 ± 24.58 %ID/g, followed by tumor at 8.63 ± 1.08 %ID/g (Fig. 5C). Subsequent biodistribution analysis data showed the same organ uptake trend as the ROI results, still having the highest renal cumulative value of 270.91 ± 39.47 %ID/g and tumor uptake of 9.71 ± 1.01 %ID/g (Fig. 5D). [^{68}Ga]Ga-NOTA-WWH347 clearly showed metastatic tumors throughout the body, encouraging us to compare its diagnostic value with the most commonly used probe, [^{18}F]F-FDG (supplementary Fig. S3D). The ROI results of [^{18}F]F-FDG showed tumor uptake of 13.13 ± 2.36 %ID/g (supplementary Fig. S3E). Although the tumor uptake of [^{68}Ga]Ga-NOTA-WWH347 was slightly lower than that of [^{18}F]F-FDG, [^{68}Ga]Ga-NOTA-WWH347 had a better tumor-to-muscle ratio (27.50 ± 15.09 vs 2.81 ± 0.56) (supplementary Fig. S3F), as well as a clearer identification of metastasis tumors on immunoPET images compared to the PET images of [^{18}F]F-FDG. The IHC results of metastatic lesions showed high expression of GPA33, which was also consistent with immunoPET imaging findings (Fig. 5E).

WWH347 is biocompatible for potential clinical applications

Finally, we evaluated the biocompatibility of WWH347 for potential clinical studies in the future. After 2 h intravenous injection, the H&E staining of major organs (including the heart, lung, liver, spleen and kidney) showed no obvious organ toxicity (supplementary Fig. S4). This suggests that WWH347 has a good prospect of clinical application due to its promising biosafety.

DISCUSSION

GPA33 is a cell surface differentiation antigen belonging to the immunoglobulin superfamily, abundantly expressed in more than 95% of human primary and metastatic CRC. Its expression is restricted in normal tissues (colon and intestinal epithelium) and not shed or secreted into the bloodstream, residing permanently in the tumor cell membranes (Ackerman *et al.* 2008). There are several studies demonstrating the feasibility of GPA33 for radioimmune-diagnostic and therapeutic purposes using radiolabeled antibodies (*e.g.*, mouse

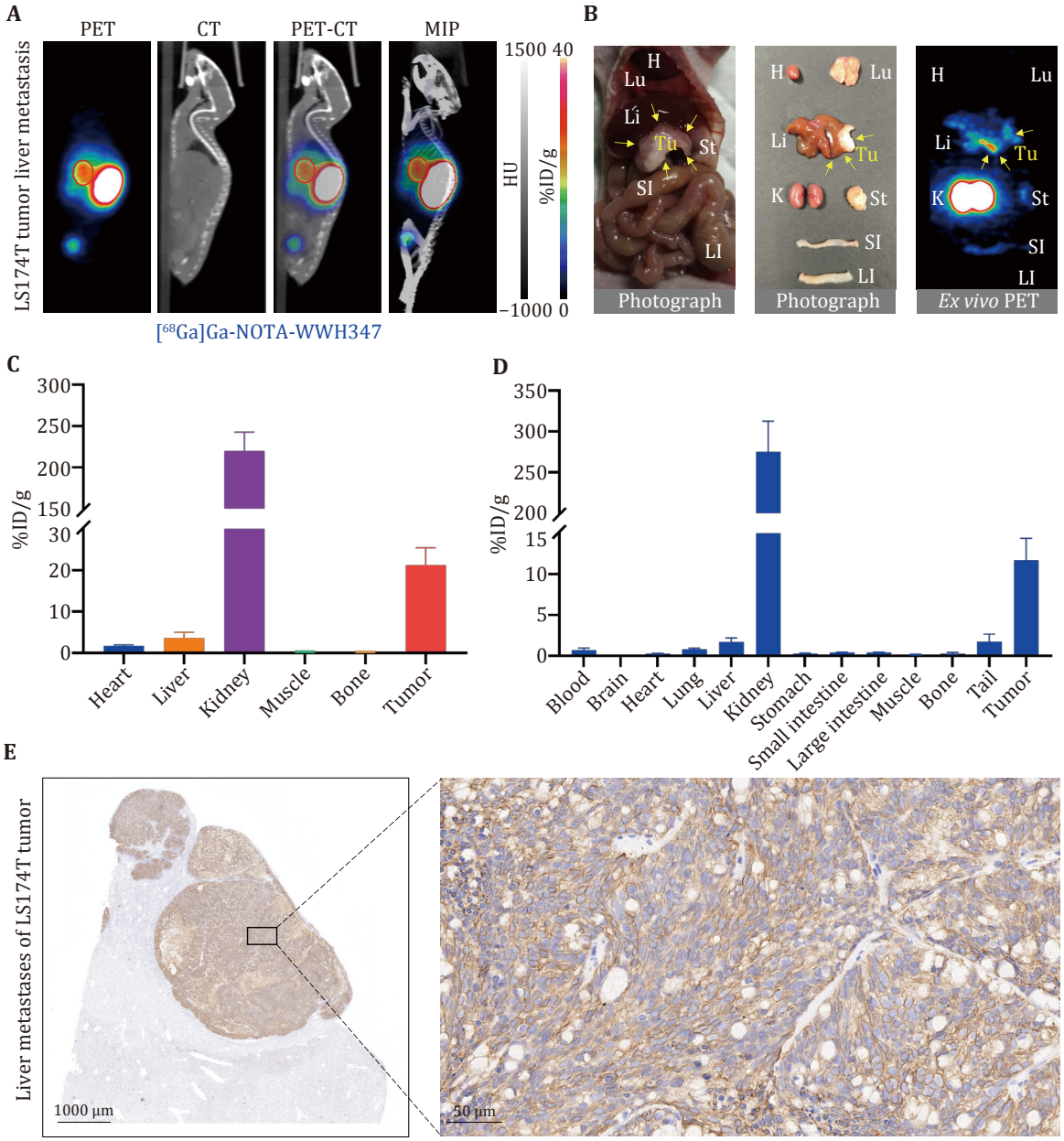

Fig. 4 ImmunoPET/CT imaging with [^{68}Ga]Ga-NOTA-WWH347 in liver metastasis LS174T tumor models. **A** Representative image of [^{68}Ga]Ga-NOTA-WWH347 (n = 4 per group) in liver metastasis LS174T tumor models. The metastatic LS174T tumor (red circles) was displayed on the coronal image and MIP image. **B** Representative anatomic diagram of liver metastasis tumor models and anatomical immunoPET/CT images of major organs. Yellow arrow: tumor. **C** ROI results in liver metastasis LS174T tumor models after 2 h of [^{68}Ga]Ga-NOTA-WWH347 injection. **D** Biodistribution results in liver metastasis LS174T models after 2 h of [^{68}Ga]Ga-NOTA-WWH347 injection. **E** IHC staining of liver metastasis of LS174T tumor. Data were quantified as %ID/g. Quantitative analysis data were shown as mean ± SD. H: heart; Lu: lung; Li: liver; K: kidney; St: stomach; SI: small intestine; LI: large intestine; Tu: tumor

monoclonal antibodies A33 and humanized antibodies huA33 (King *et al*. 1995). GPA33-targeted nuclear imaging tools can be used for diagnosing and treating GPA33-positive tumors, screening patients for GPA33-targeted therapies and monitoring therapeutic outcomes. Vaughn *et al*. imaged and treated a preclinical model of CRC using a ^{177}Lu-labelled monoclonal antibody (Vaughn *et al*. 2024). Cheal *et al*. demonstrated that ^{86}Y and ^{177}Lu-labelled bispecific antibodies showed favorable therapeutic results (Cheal *et al*. 2016). However, the long circulation time of large-sized antibodies, which requires the use of long half-life radionuclides

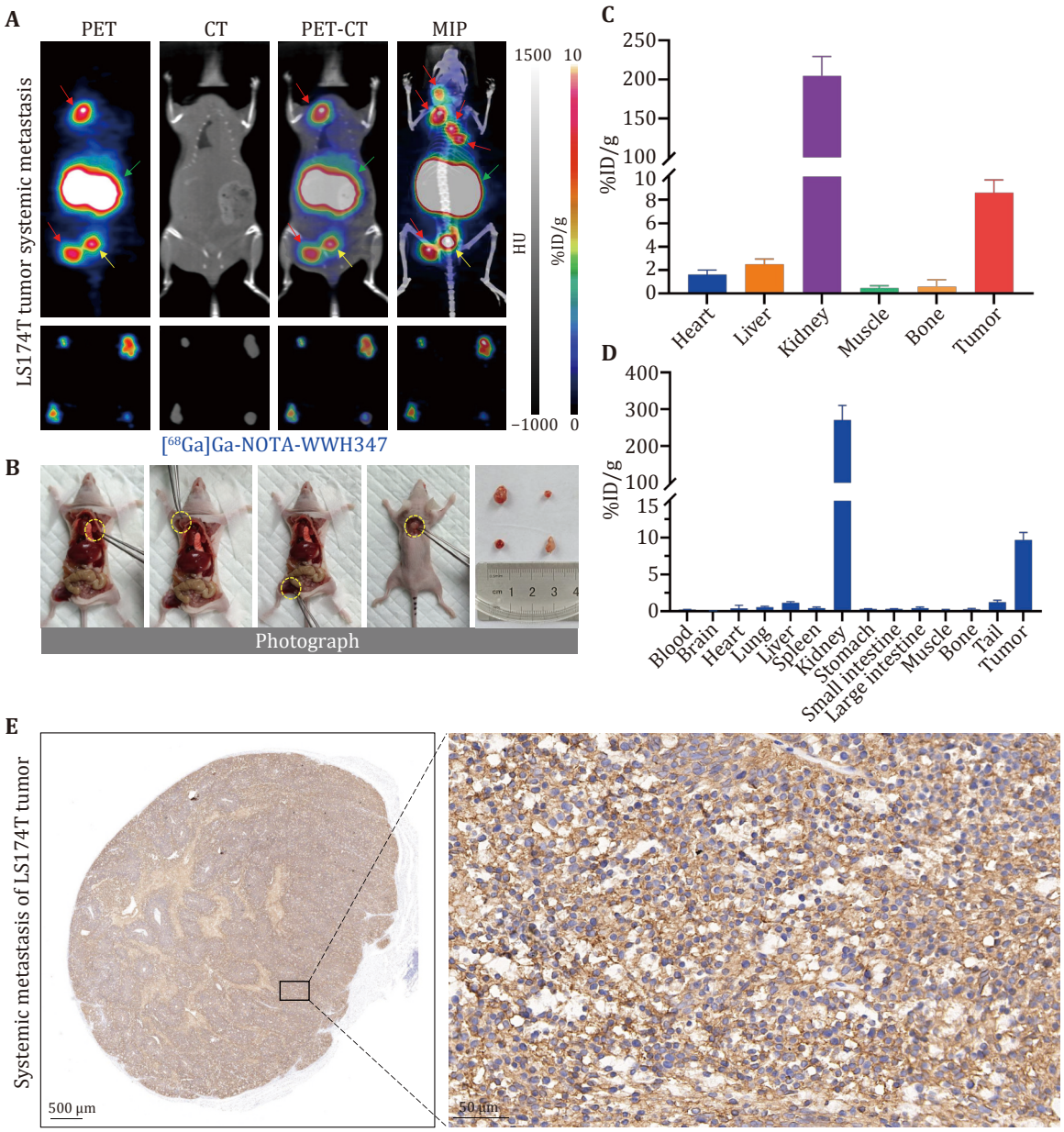

Fig. 5 ImmunoPET/CT imaging with [^{68}Ga]Ga-NOTA-WWH347 in systemic metastasis LS174T tumor models. **A** Representative image of [^{68}Ga]Ga-NOTA-WWH347 (n = 6 per group) in systemic metastasis LS174T tumor models. The metastatic LS174T tumor (red arrows), the kidneys (green arrows) and bladders (yellow arrows) were displayed on the coronal image and MIP image. **B** Representative anatomic diagram of systemic metastasis tumor models. Yellow circle: tumor. **C** ROI quantification in systemic metastasis LS174T tumor models after 2 h of [^{68}Ga]Ga-NOTA-WWH347 injection. **D** Biodistribution results in systemic metastasis LS174T models after 2 h of [^{68}Ga]Ga-NOTA-WWH347 injection. **E** IHC staining of systemic metastasis of LS174T tumor. Data were quantified as %ID/g. Quantitative analysis data were shown as mean ± SD

for immunoimaging, limits their use in clinical practice (Chames *et al*. 2009). Nanobodies, on the other hand, as the smallest type of antibody derivative, have the same antigen recognition structure as monoclonal antibodies with low immunogenicity. Compared to these antibody-based approaches, our nanobody tracer offers distinct advantages in pharmacokinetics and imaging efficiency. When benchmarked against other CRC imaging probes, [^{68}Ga]Ga-NOTA-WWH347 demonstrates superior target specificity compared to metabolic tracers like [^{18}F]F-FDG, and faster tumor penetration than antibody-based agents. In addition, their diameter of less than 4 nm allows them to penetrate deeper into tumor tissues while retaining their antigen recognition ability

(Ackaert *et al*. 2021). More importantly, rapid clearing of nanobodies from the circulation allows the short half-life radionuclide-labelled probes to be used for same-day imaging for diagnostic purposes (Krasniqi *et al*. 2018).

In this study, we synthesized an innovative GPA33-targeted immunoPET nanobody tracer, which can be used not only as a colorectal tumor visualizer for diagnosis, staging, and prognosis, but also for screening patients who may benefit from GPA33-targeted therapy. Consistent with clinical priorities for metastasis detection, the tracer achieved tumor-to-muscle ratios >27 in metastatic lesions — significantly surpassing [^{18}F]F-FDG's performance (2.81 ± 0.56) in the same models. This high contrast is critical for detecting small peritoneal implants and occult abdominal metastases. However, prominent kidney accumulation was observed — a common challenge with low-molecular-weight tracers like nanobodies that may obscure abdominal metastases and raise nephrotoxicity concerns. To address renal retention, several effective strategies have been proposed. Zhou *et al*. reduced kidney retention in radiolabeled sdAbs by incorporating renal brush border enzyme-cleavable linkers (*e.g*., GK-type) into prosthetic groups. These linkers, attached via click chemistry, enable enzymatic cleavage in proximal tubules, facilitating urinary excretion of radiolabeled fragments and significantly lowering renal uptake while preserving tumor targeting (Zhou *et al*. 2018, 2021). Wang *et al*. reduced kidney retention of the CD38-targeted probe [^{68}Ga]Ga-NOTA-Nb1053 by implementing pharmaceutical premedication with either sodium maleate or fructose prior to probe administration, which significantly decreased kidney uptake and improved the diagnostic value of the probe (Wang *et al*. 2021). Xenaki *et al*. reduced kidney retention of the HER2-targeted nanobody 11A4 by genetically fusing it to an albumin-binding domain (ABD), which extended serum half-life and redirected clearance pathways, resulting in reduced renal accumulation while maintaining homogenous tumor distribution (Xenaki *et al*. 2021).

This study has several limitations that require further research. This study acknowledges several limitations. Primarily, the sensitivity of the tracer for detecting early-stage CRC requires validation in dedicated clinical studies. Secondly, the clinical safety and efficacy profile must be further established in larger, more diverse patient cohorts. A significant challenge for clinical translation is the observed renal retention of the tracer, which necessitates optimization to reduce renal exposure. Critically, it is important to note that there are currently no clinically approved diagnostic or therapeutic agents targeting GPA33, highlighting the unmet medical need and the potential significance of this approach. To address this gap and advance the field, our research group is committed to advancing the clinical development of WWH347, our GPA33-targeting nanobody tracer. Future research directions will focus on: conducting clinical trials to rigorously correlate PET imaging findings with GPA33 expression levels in early-stage CRC tissues; exploring the theranostic potential of pairing this tracer platform with the therapeutic radionuclide ^{177}Lu for targeted radiotherapy; and engineering next-generation variants of the tracer with significantly reduced renal uptake through protein engineering strategies to enhance its clinical translation potential.

In summary, we successfully synthesized the GPA33-targeted nanobody tracer [^{68}Ga]Ga-NOTA-WWH347, demonstrating its potential as a precision immunoPET tool for colorectal cancer. The probe exhibits high specificity, rapid tumor penetration, and generates exceptional tumor-to-background contrast — crucial for detecting metastases — while enabling same-day imaging. However, prominent renal retention remains a translational challenge requiring optimization. Despite this limitation and the current absence of clinically approved GPA33-targeted agents, this tracer represents a significant step towards noninvasive visualization of GPA33 expression dynamics. This capability is essential for advancing GPA33-targeted therapeutics, facilitating patient stratification, treatment monitoring, and ultimately, personalized management of colorectal cancer.

MATERIALS AND METHODS

Cell culture and animal models

CRC cell lines (LS174T, HT29) were obtained from Procell Life Science & Technology (Wuhan, China). LS174T cells were cultured in DMEM medium (Gibco; Grand Island, NY), and HT29 cells were cultured in McCoy's 5A medium (Gibco; Grand Island, NY). Both cell lines were supplemented with 10% fetal bovine serum (FBS; Gibco Grand Island, NY) and 1% penicillin/streptomycin (Procell; Wuhan) and cultured at 37°C with 5% CO_2.

All animal experiments followed the Institutional Animal Care and Use Committee of Huazhong University of Science and Technology-approved protocol. Female BALB/c nude mice (4–6 weeks old) were provided by Beijing Vital River Laboratory Animal Technology Co., Ltd. (Beijing, China). For subcutaneous

tumor models, 5×10^6 tumor cells were resuspended in sterile phosphate-buffered saline (PBS, Gibco) and then implanted into the right axilla of each mouse. The subcutaneous tumor models were used for immunoPET imaging when the cells were implanted for about two weeks, and the average diameter reached 0.6–1.0 cm. For liver metastasis LS174T tumor models, 5×10^5 LS174T cells were resuspended in 100 μL sterile PBS (Gibco) and then mice were continuously anesthetized with a small animal gas anesthesia system (2% isoflurane), the skin was incised at the projection area of the spleen body surface, the spleen was exposed, and the needle was inserted with a syringe under the dorsal membrane of the spleen from the proximity to the lower pole of the spleen and 100 μL of the LS174T cells were injected slowly, and the syringe was withdrawn after a period of time to ligate the blood vessels connecting to the spleen and resect the spleen, and the abdomen was closed layer by layer. The liver metastasis LS174T tumor models were used for immunoPET imaging when the cells were implanted for about four weeks. For system metastasis LS174T tumor models, 5×10^6 LS174T cells were resuspended in sterile PBS (Gibco) and injected into mice via the tail vein. The system metastasis LS174T tumor models were used for immunoPET imaging when the cells were implanted for about three weeks.

Western blot

LS174T and HT29 cells were cultured in Petri dishes, and total protein was extracted when the cells grew to 75%~80%. The protein concentration was determined by bicinchoninic acid assay (BCA) kit (Biosharp, china), and Sodium dodecyl sulfate-polyacrylamide gel electrophoresis (SDS-PAGE) was carried out. After electrophoresis, the membrane was transferred to and closed PVDF membrane. Recombinant Anti-GPA33 antibody (ab108938, Abcam; Wuhan, China) was chosen as the primary antibody. The Anti-GPA33 antibody was diluted at 1:1,000, and then incubated with the PVDF membrane at 4°C overnight. Then it was incubated with HRP-conjugated goat anti-rabbit IgG secondary antibody (Jackson ImmunoResearch Laboratories Inc., USA) at room temperature on the shaker for 2 h and developed. The gray value of the bands was determined by Image J software.

Production and radiolabeling of nanobodies

A novel anti-human GPA33 nanobody (*i.e.*, WWH347) and a non-specific nanobody (*i.e.*, A50-2_5D5) were generated through a series of steps of immunization of alpacas with recombinant human GPA33 protein, library construction, phage display, high-throughput sequencing, and recombinant expression in Chinese hamster ovary (CHO) cells. SDS-PAGE and high-performance liquid chromatography (HPLC) were used to detect the protein expression and purity. The purity was evaluated by densitometric analysis after the Coomassie blue staining of SDS-PAGE gels under reducing and non-reducing conditions.

The nanobodies were conjugated with the bi-functional chelator 2-S-(4-Isothiocyanatobenzyl)-1,4,7-triazacyclononane-1,4,7-triacetic acid (p-SCN-Bn-NOTA; Macrocyclics) for subsequent ^{68}Ga-labelling. Briefly, 1 mg of nanobodies in PBS solvent was adjusted to pH 9.0–10.0 by adding 0.1 mol/L Na_2CO_3 buffer. P-SCN-Bn-NOTA (dissolved in DMSO, 20 equivalents) was added to the solution and reacted overnight at room temperature away from light for 2 h, followed by purification using equilibrated PD-10 desalting columns (Cytia, USA) to remove excess p-SCN-Bn-NOTA and concentration using 10 kDa ultrafiltration tubes (Millipore). The conjugated nanobodies were stored at −20°C for subsequent radiolabeling applications. 4 mCi ^{68}Ga eluted with 0.1 mol/L hydrogen chloride (pH = 1) from a germanium-gallium generator was used for radiolabeling, and the pH was adjusted to 4.0–4.5 with 0.5 mol/L sodium acetate (pH = 5). Subsequently, previously conjugated NOTA-nanoantibodies were added. The solution was continuously shaken at 37°C (400 r/min) for 15 min. The final radioactive product was purified with a sterile PBS mobile phase using an equilibrated PD-10 column. The radiochemical purity of the final product was evaluated by HPLC. Instant thin-layer chromatography (iTLC, Agilent Technologies Inc.) was used to detect the stability of the probe serum after co-incubation with 50% FBS at 37°C for gradient time (including 5 min, 15 min, 30 min, 45 min, 1 h, 1.5 h, 2 h, 3 h, and 4 h).

Cell uptake

LS174T and HT29 cells were seeded in 24-well plates, incubated for 24 h and then added with 0.074 MBq of [^{68}Ga]Ga-NOTA-WWH347 per well, respectively. The cells were incubated at 37°C for 15, 30, 60, and 120 min. For *in vitro* blocking experiments, cells were co-incubated with 10 μg of nanobody precursor. After incubation, these cells were washed, collected and measured with the gamma counter (WIZARD 2480, PekinElmer).

ImmunoPET imaging

3.7 MBq of [^{68}Ga]Ga-NOTA-WWH347 and [^{68}Ga]Ga-NOTA-A50-2_5D5 were administered to the mice

bearing subcutaneous LS174T CRC cell-derived xenograft (CDX). 3.7 MBq of [^{68}Ga]Ga-NOTA-WWH347 were also administered to the liver metastasis LS174T tumor models and system metastasis LS174T tumor models. The mice were anaesthetized and placed in the prone position in the scanning bed 2 h after injection. All images were acquired by the Trans-PET IMAGING SYSTEM (Trans-PET Discoverist 180, Suzhou Ruipaining Technology Co., ltd, Jiangsu, China). Maximum intensity projection (MIP) and transaxial images were shown using the Inveon Research Workplace (Siemens Preclinical Solutions). For quantitative analysis, regions of interest (ROIs) of main organs and tumors were delineated on selected transaxial images, and the radioactive counts were presented in terms of percentage dose rate per gram of tissue (%ID/g).

Ex vivo biodistribution and histopathological study

The *ex vivo* biodistribution studies were performed at 2 h post-injection to quantify the uptake of radiolabeling probes in organs/tissues. The mice were euthanized, and multiple organs/tissues (including the blood, brain, heart, lung, liver, spleen, kidney, stomach, small intestine, large intestine, muscle, bone, and tumor) were collected and wet-weighed. The radioactivity of organs/tissues was quantified by the gamma counter (WIZARD 2480, PekinElmer). The biodistribution data were represented as %ID/g after attenuation correction.

Isolated tumor tissue was fixed with paraformaldehyde tissue fixative after radioactive counting. Immunohistochemical (IHC) staining was performed using GPA33 (ab108938, Abcam) according to standard protocols.

[^{18}F]F-FDG PET imaging

Each mouse was injected with 3.7 MBq of [^{18}F]F-FDG into the lateral tail vein and maintained under isoflurane anesthesia for 2 h, with body temperature maintained with a heating pad, prior to PET imaging. For quantitative analysis, the ROI was plotted as %ID/g.

Biosafety assessment of WWH347

To assess the biosafety of WWH347 and saline as a control, the healthy BALB/c mice were randomly divided into two groups. Specifically, WWH347 and an equal volume of saline were injected via the tail vein. The mice were euthanized after 2 h. The major retention and metabolizing organs (heart, lung, liver, spleen and kidney) were dissociated, sectioned and stained with hematoxylin-eosin (H&E) solution. Images were taken under the microscope.

Statistical analysis

Statistical analysis and charting were performed by the GraphPad Prism software (version 9.5, USA). All data were shown as mean ± SD. Statistical analysis was performed using the unpaired Student's *t*-test. Differences were considered statistically significant when *P*-values were <0.05.

Acknowledgements The authors are grateful for the financial support by the National Key Research and Development Program of China (2022YFB3808200), National Institutes of Health (P30CA014520) and Open Program of Hubei Province Key Laboratory of Molecular Imaging (2024fzyx014).

Compliance with Ethical Standards

Conflict of interest Weibo Cai declares conflict of interest with the following corporations: Portrai, Inc., rTR Technovation Corporation, and Four Health Global Pharmaceuticals Inc. Chengwen Zheng, Zhidie Huang, Shaowen Yang, Sixuan Cheng, Wenbo Li, Hao Yang, Dawei Jiang, and Weijun Wei declare that they have no conflict of interest.

Human and animal rights and informed consent This article does not contain any studies with human subjects performed by any of the authors. For animal studies, all institutional and national guidelines for the care and use of laboratory animals were followed.

References

Abakushina EV, Gelm YV, Pasova IA, Bazhin AV (2019) Immunotherapeutic approaches for the treatment of colorectal cancer. Biochemistry (Moscow) 84(7): 720–728

Abedizadeh R, Majidi F, Khorasani HR, Abedi H, Sabour D (2024) Colorectal cancer: a comprehensive review of carcinogenesis, diagnosis, and novel strategies for classified treatments. Cancer Metastasis Rev 43(2): 729–753

Ackaert C, Smiejkowska N, Xavier C, Sterckx YGJ, Denies S, Stijlemans B, Elkrim Y, Devoogdt N, Caveliers V, Lahoutte T,

Muyldermans S, Breckpot K, Keyaerts M (2021) Immunogenicity risk profile of nanobodies. Front Immunol 12: 632687. https://doi.org/10.3389/fimmu.2021.632687

Ackerman ME, Chalouni C, Schmidt MM, Raman VV, Ritter G, Old LJ, Mellman I, Wittrup KD (2008) A33 antigen displays persistent surface expression. Cancer Immunol Immunother 57(7): 1017–1027

Ametamey SM, Honer M, Schubiger PA (2008) Molecular imaging with PET. Chem Rev 108(5): 1501–1516

Bendell JC, Lenz H-J, Ryan T, El-Rayes BF, Marshall JL, Modiano MR, Hart LL, Kingsley CD, George TJ, Nakashima D, Berlin JD (2014) Phase 1/2 study of KRN330, a fully human anti-A33 monoclonal antibody, plus irinotecan as second-line treatment for patients with metastatic colorectal cancer. Invest New Drugs 32(4): 682–690

Carrasquillo JA, Pandit-Taskar N, O'Donoghue JA, Humm JL, Zanzonico P, Smith-Jones PM, Divgi CR, Pryma DA, Ruan S, Kemeny NE, Fong Y, Wong D, Jaggi JS, Scheinberg DA, Gonen M, Panageas KS, Ritter G, Jungbluth AA, Old LJ, Larson SM (2011) ^{124}I-huA33 antibody PET of colorectal cancer. J Nucl Med 52(8): 1173–1180

Chames P, Van Regenmortel M, Weiss E, Baty D (2009) Therapeutic antibodies: successes, limitations and hopes for the future. Br J Pharmacol 157(2): 220–233

Chandler CS, Bell MM, Chung SK, Veach DR, Fung EK, Punzalan B, Vargas DB, PatelM, Xu H, Guo H-F, Santich BH, Zanzonico PB, Monette S, Nash GM, Cercek A, Jungbluth A, Pandit-Taskar N, Cheung NKV, Larson SM, Cheal SM (2022) Intraperitoneal pretargeted radioimmunotherapy for colorectal peritoneal carcinomatosis. Mol Cancer Ther 21(1): 125–137

Cheal SM, Xu H, Guo H-F, Lee S-G, Punzalan B, Chalasani S, Fung EK, Jungbluth A, Zanzonico PB, Carrasquillo JA, O'Donoghue J, Smith-Jones PM, Wittrup KD, Cheung N-KV, Larson SM (2016) Theranostic pretargeted radioimmunotherapy of colorectal cancer xenografts in mice using picomolar affinity ^{86}Y- or ^{177}Lu-DOTA-bn binding scFv C825/GPA33 IgG bispecific immunoconjugates. Eur J Nucl Med Mol Imaging 43(5): 925–937

Chong G, Lee FT, Hopkins W, Tebbutt N, Cebon JS, Mountain AJ, Chappell B, Papenfuss A, Schleyer P, U P, Murphy R, Wirth V, Smyth FE, Potasz N, Poon A, Davis ID, Saunder T, O'Keefe GJ, Burgess AW, Hoffman EW, Old LJ, Scott AM (2005) Phase I trial of ^{131}I-huA33 in patients with advanced colorectal carcinoma. Clin Cancer Res 11(13): 4818–4826

Eng C, Jácome AA, Agarwal R, Hayat MH, Byndloss MX, Holowatyj AN, Bailey C, Lieu CH (2022) A comprehensive framework for early-onset colorectal cancer research. Lancet Oncol 23(3): e116–e128

Fenster A, Downey DB (2000) Three-dimensional ultrasound imaging. Annu Rev Biomed Eng 2: 457–475

Flohr T, Schmidt B (2023) Technical basics and clinical benefits of photon-counting CT. Invest Radiol 58(7): 441–450

Ganesh K, Stadler ZK, Cercek A, Mendelsohn RB, Shia J, Segal NH, Diaz LA Jr (2019) Immunotherapy in colorectal cancer: rationale, challenges and potential. Nat Rev Gastroenterol Hepatol 16(6): 361–375

Garinchesa P, Sakamoto J, Welt S, Real F, Rettig W, Old L (1996) Organ-specific expression of the colon cancer antigen A33, a cell surface target for antibody-based therapy. Int J Oncol 9(3): 465–471

Grilo AL, Mantalaris A (2019) The increasingly human and profitable monoclonal antibody market. Trends Biotechnol 37(1): 9–16

Heath JK, White SJ, Johnstone CN, Catimel B, Simpson R, Moritz R, Tu G-F, Ji H, Whitehead R, Groenen L, Scott A, Ritter G, Cohen L, Welt S, Old L, Nice E, Burgess A (1997) The human A33 antigen is a transmembrane glycoprotein and a novel member of the immunoglobulin superfamily. Proc Natl Acad Sci USA 94(2): 469–474

Heriot AG, Grundy A, Kumar D (1999) Preoperative staging of rectal carcinoma. Br J Surg 86(1): 17–28

Infante JR, Bendell JC, Goff LW, Jones SF, Chan E, Sudo T, Burris HA, Berlin JD (2013) Safety, pharmacokinetics and pharmacodynamics of the anti-A33 fully-human monoclonal antibody, KRN330, in patients with advanced colorectal cancer. Eur J Cancer 49(6): 1169–1175

James ML, Gambhir SS (2012) A molecular imaging primer: modalities, imaging agents, and applications. Physiol Rev 92(2): 897–965

King DJ, Antoniw P, Owens RJ, Adair JR, Haines AMR, Farnsworth APH, Finney H, Lawson ADG, Lyons A, Baker TS, Baldock D, Mackintosh J, Gofton C, Yarranton GT, McWilliams W, Shochat D, Leichner PK, Welt S, Old LJ, Mountain A (1995) Preparation and preclinical evaluation of humanised A33 immunoconjugates for radioimmunotherapy. Br J Cancer 72(6): 1364–1372

Krasniqi A, D'Huyvetter M, Devoogdt N, Frejd FY, Sörensen J, Orlova A, Keyaerts M, Tolmachev V (2018) Same-day imaging using small proteins: clinical experience and translational prospects in oncology. J Nucl Med 59(6): 885–891

Lopes N, Bergsland C, Bruun J, Bjørnslett M, Vieira AF, Mesquita P, Pinto R, Gomes R, Cavadas B, Bennett E, Pereira E, Lothe RA, Almeida R, David L (2020) A panel of intestinal differentiation markers (CDX2, GPA33, and LI-cadherin) identifies gastric cancer patients with favourable prognosis. Gastric Cancer 23(5): 811–823

Menzies AM, Lastoria S (2022) PET imaging for cancer immunotherapy: the immuno-PET. Ann Oncol 33(1): 13–14

Schwab KE, Gailloud P, Wyse G, Tamargo RJ (2008) Limitations of magnetic resonance imaging and magnetic resonance angiography in the diagnosis of intracranial aneurysms. Neurosurgery 63(1): 29–35

Siegel RL, Wagle NS, Cercek A, Smith RA, Jemal A (2023) Colorectal cancer statistics, 2023. CA Cancer J Clin 73(3): 233–254

Tan H, Gu Y, Yu H, Hu P, Zhang Y, Mao W, Shi H (2020) Total-body PET/CT: current applications and future perspectives. AJR Am J Roentgenol 215(2): 325–337

Ulintz PJ, Greenson JK, Wu R, Fearon ER, Hardiman KM (2018) Lymph node metastases in colon cancer are polyclonal. Clin Cancer Res 24(9): 2214–2224

Vaughn BA, Lee SG, Vargas DB, Seo S, Rinne SS, Xu H, Guo H-F, Le Roux AB, Gajecki L, Krebs S, Yang G, Ouerfelli O, Zanzonico PB, Fung EK, St. Jean S, Carrasco SE, Jungbluth A, Cheung NKV, Larson SM, Veach DR, Cheal SM (2024) Theranostic GPA33-pretargeted radioimmunotherapy of human colorectal carcinoma with a bivalent ^{177}Lu-labeled radiohapten. J Nucl Med 65(10): 1611–1618

Wang C, Chen Y, Hou YN, Liu Q, Zhang D, Zhao H, Zhang Y, An S, Li L, Hou J, Huang G, Liu J, Zhao YJ, Wei W (2021) ImmunoPET imaging of multiple myeloma with [^{68}Ga]Ga-NOTA-Nb1053. Eur J Nucl Med Mol Imaging 48(9): 2749–2760

Wang X-Y, Yang F, Jin C, Fu D-L (2014) Utility of PET/CT in diagnosis, staging, assessment of resectability and metabolic response of pancreatic cancer. World J Gastroenterol 20(42): 15580–15589

Wei W, Rosenkrans ZT, Liu J, Huang G, Luo Q-Y, Cai W (2020) ImmunoPET: concept, design, and applications. Chem Rev 120(8): 3787–3851

Wei W, Younis MH, Lan X, Liu J, Cai W (2022) Single-domain antibody theranostics on the horizon. J Nucl Med 63(10):

1475–1479
Weissleder R (2006) Molecular imaging in cancer. Science 312(5777): 1168–1171
Welt S, Scott AM, Divgi CR, Kemeny NE, Finn RD, Daghighian F, Germain JS, Richards EC, Larson SM, Old LJ (1996) Phase I/II study of iodine 125-labeled monoclonal antibody A33 in patients with advanced colon cancer. J Clin Oncol 14(6): 1787–1797
Welt S, Ritter G, Williams C Jr, Cohen LS, John M, Jungbluth A, Richards EA, Old LJ, Kemeny NE (2003) Phase I study of anticolon cancer humanized antibody A33. Clin Cancer Res 9(4): 1338–1346
Xenaki KT, Dorresteijn B, Muns JA, Adamzek K, Doulkeridou S, Houthoff H, Oliveira S, Van Bergen en Henegouwen PM (2021) Homogeneous tumor targeting with a single dose of HER2-targeted albumin-binding domain-fused nanobody-drug conjugates results in long-lasting tumor remission in mice. Theranostics 11(11): 5525–5538
Zhou Z, Devoogdt N, Zalutsky MR, Vaidyanathan G (2018) An efficient method for labeling single domain antibody fragments with ^{18}F using tetrazine-*Trans*-cyclooctene ligation and a renal brush border enzyme-cleavable linker. Bioconjug Chem 29(12): 4090–4103
Zhou Z, Meshaw R, Zalutsky MR, Vaidyanathan G (2021) Site-specific and residualizing linker for ^{18}F labeling with enhanced renal clearance: application to an anti-HER2 single-domain antibody fragment. J Nucl Med 62(11): 1624–1630